IEEE Access
Multidisciplinary ⋮ Rapid Review ⋮ Open Access Journal

Received 24 February 2024, accepted 6 March 2024, date of publication 18 March 2024, date of current version 16 April 2024.

Digital Object Identifier 10.1109/ACCESS.2024.3376392

RESEARCH ARTICLE

Hybrid Control Method of Full-Bridge LLC Resonant Converter Based on Electric Vehicle

YUNTAO YUE, YUFAN LIU, JIARAN ZHANG, HONGWEI ZHAO, AND JIN YANG
School of Electrical and Information Engineering, Beijing University of Civil Engineering and Architecture, Beijing 100044, China

Corresponding author: Yuntao Yue (yueyuntao@bucea.edu.cn)

ABSTRACT The high charging efficiency of LLC resonant converters over a very wide range of load conditions in electric vehicle charging systems has long been a research hotspot. In this paper, a hybrid control method is proposed for LLC resonant converter by combining pulse width modulation (PWM) and burst control to address the issues of small excitation current and limited output voltage range under the light load condition. The resonant current energy in the burst-on period is used to supplement the missing excitation current energy from PWM control zero voltage switching to realize PWM-Burst control. Therefore, a hybrid control of PFM and PWM-Burst is employed for LLC resonant converters under full load conditions. The proposed hybrid control method focuses on steady-state operation, and its operating principles are introduced and analyzed. Finally, simulation and experiments were conducted through Matlab-Simulink to verify the feasibility of the proposed method, and a 1-kW laboratory prototype was constructed to validate the effectiveness and advantages of the proposed method.

INDEX TERMS Burst control, electric vehicle, LLC resonant converter, PFM control, PWM control.

I. INTRODUCTION

In the past decade, there has been a significant surge in the adoption of electric vehicles to combat the reliance on fossil fuels, a crucial step towards achieving carbon neutrality [1]. Consequently, this has sparked a notable growth in the electric vehicle charger market and a strong desire to enhance charging efficiency. The DC-DC converter, an integral part of the electric vehicle charger, requires further optimization to meet these demands.

The DC-DC converter has a very wide range of input voltage, but it requires a high efficiency to work at nominal input voltage [2]. Therefore, it is necessary to improve the efficiency of the DC-DC converter under light load at nominal input voltage [3], [4]. When using the traditional DC-DC converter in electric vehicle charging systems, there are problems such as large current stress and power return. However, these problems can be solved by adding an LLC resonant cavity to the DC-DC converter, and the function of step-up and step-down is realized according to the actual charging voltage [5], [6], [7]. Due to their desirable characteristics such as high efficiency and reliability, LLC resonant converters are considered an attractive power architecture in electric vehicle charging systems and have been thoroughly studied in the literatures [8] and [9]. The current mainstream LLC resonant converter is a bidirectional converter [10], [11], but in the case of electric vehicle charging, energy is not required to complete bidirectional flow. Thus, in this paper, rectifier diodes are used for secondary-side full bridge switch tubes to greatly save device resources. It has been extensively studied and implemented in practical applications.

Generally, pulse frequency modulation (PFM) is employed in LLC converters, but the limited operating frequency range of the converter restricts the attainment of wide-range voltage regulation. Therefore, most conventional LLC topologies are used in dc converters with a small input or output range. With the expansion of the application domain, LLC converters with wide input or output ranges have emerged as a new research field [12]. To achieve a wide voltage output range for LLC converters within a limited operating frequency,

The associate editor coordinating the review of this manuscript and approving it for publication was Junho Hong.

various methods have been proposed from different aspects of circuit design. Optimizing the driving signal modulation is a significant approach to increasing the output voltage range. Typically, based on PFM control, pulse width modulation (PWM), phase-shift modulation (PSM), and burst-mode control can be added. Although these control methods have been widely used in other types of converters, some new issues arise when they are applied to LLC converters.

In [13], a hybrid control strategy combining PWM with PFM was investigated to achieve a lower voltage gain under light load conditions. However, the soft-switching performance was not improved, resulting in output voltage constraint. PSM control has been widely adopted in LLC converters to reduce transformer core losses and adjust the output voltage under light load conditions [8], [14], [15], [16]. However, when the phase-shift angle is large, the soft-switching performance of the lagging bridge arm may be affected. Moreover, when the circuit operates under light load conditions, this may impact the reliability of the converter operation. In [17] and [18], PSM was used as a supplementary control strategy for PFM to achieve a wide gain range. In [19] and [20], phase-shedding methods were proposed, which enhance light load efficiency by reducing the number of devices. However, phase shedding can only be applied to multiple transformer systems. Burst control converts the output voltage of the switch array from continuous mode to discontinuous mode [21], [22], which decreases the equivalent input voltage of the resonant cavity and thus reduces the output voltage. However, burst control will also increase the output ripple, making the electromagnetic interference (EMI) characteristics of the system worse [23]. In the burst-on period, the resonant current decreases when the output voltage increases, and vice versa. When the resonant current increases, the resonant inductor and the magnetic flux of the excitation inductor will increase, thus, the output voltage ripple and loss will increase. This phenomenon is especially obvious when the output voltage is low, which affects the converter conversion efficiency under light load.

Through the analysis of PWM control and Burst control, it can be observed that:

1. The decrease of duty cycle follows the decrease of excitation current of PWM control, which cannot provide all the energy required for zero voltage switching (ZVS) of the switching tube under light load;

2. Similarly, the resonant current of burst control is too large to achieve high conversion efficiency in this system.

Therefore, in this paper, a hybrid control method combining PWM and burst control is proposed to make the PWM comparator generate PWM pulses in the burst-on period. By harnessing the excessive resonant current during the turn-on period, the PWM control is empowered to achieve ZVS, thus addressing the limitation of insufficient excitation current in conventional PWM control. Furthermore, the hybrid approach allows for the conversion of a portion of the burst control's energy into PWM control, leading to a reduction in both the energy consumption on the secondary side and the output voltage ripple. This innovation enhances the EMI performance and broadens the output voltage spectrum.

II. PROPOSED LLC RESONANT CONVERTER

A. CIRCUIT CONFIGURATION

The topological structure of the full-bridge LLC resonant converter is shown in Figure 1. The full-bridge inverter is composed of four power MOS tubes; the resonant cavity is composed of a resonant inductor L_r, a resonant capacitor C_r and a magnetizing inductor Lr; the secondary side of the transformer is a full bridge rectifier structure; C_o is connected in parallel with the full-bridge rectifier structure for filtering, and finally, the DC output voltage is obtained.

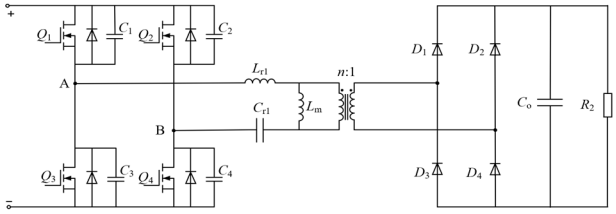

FIGURE 1. Full-bridge LLC resonant converter topology.

When the input terminal is connected to the rated voltage, the full-bridge inverter circuit converts the rated voltage into positive and negative input voltage. Q_1 and Q_3, Q_2 and Q_4 are complementary frequency modulations used to control the switch network of the converter, with the switching frequency of the power tube considered as the operating frequency [12]. The resonance inductance Lr, resonance capacitance Cr, and magnetizing inductance Lm together form a resonant cavity. The rectifier filter circuit diode is turned on and off based on the direction of the secondary current, and the parallel structure with the filter capacitor allows for more precise filtering of the high-frequency or low-frequency AC portion of the DC output voltage. Finally, the DC output voltage required to power the load is obtained.

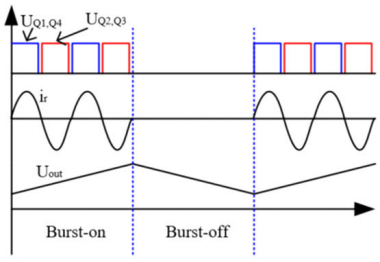

FIGURE 2. Typical waveform of Burst control.

III. OPERATION PRINCIPLE

A. BURST INTERMITTENT CONTROL

Burst control, also known as intermittent control, is a control method to reduce switching losses so that the switch tube is in periodic conduction. During the switching tube-off time, the energy can be stored by energy storage components such as

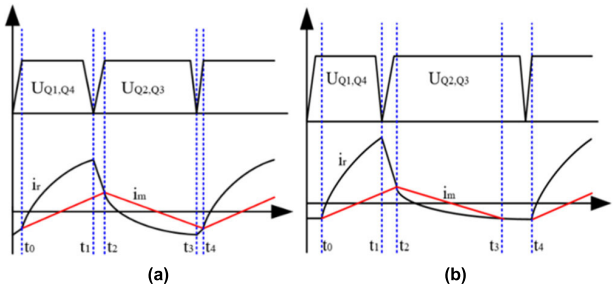

FIGURE 3. PWM control waveform.

the switching tube junction capacitor to provide the energy required for operation during the turn-on time. A typical waveform is shown in Figure 2.

Defining the duty cycle of burst control as D_{burst}, the resonant current during the burst-on period can be expressed as [23]:

$$i_{rl}(t) = \frac{U_{inl}(t) - U_{outl}(t)}{jX_r} \tag{1}$$

where: $i_{r1}(t)$ denotes the fundamental component of the resonant current;

$U_{in1}(t)$ denotes the fundamental component of the input voltage;

$U_{out1}(t)$ denotes the fundamental component of the output voltage.

X_r denotes the resonant cavity equivalent reactance.

The equivalent reactance of the resonant cavity is expressed as:

$$X_r = \omega_s L_r - \frac{1}{\omega_s C_r} \tag{2}$$

From Eq. (2), X_r varies positively with the switching frequency ω_s, but since there is a maximum value of frequency ω_s, X_r does not grow indefinitely, and the same maximum value exists; also, X_r is related to the resonant parameters of the converter, and increasing ω_s or the value of resonant parameters can reduce the equivalent impedance of the resonant cavity. Combined with (1), the resonant current decreases with the growth of the output voltage during the burst-on period, and vice versa. When i_r becomes larger, the voltage across the resonant capacitor increases, while the resonant inductance and excitation inductance flux increase, which will increase output voltage ripple and losses after transformer conversion to the secondary side. This phenomenon is especially obvious at low output voltage, which affects the conversion efficiency of the converter under a light load.

B. PWM CONTROL

There are two typical waveforms for PWM control, as shown in Figure 3.

The first one is when the switching tubes Q_2 and Q_3 are off, i.e., the t3∼t4 period. At this time, the excitation current is larger than the resonant current, and the duty cycle is larger. The second one is the t3∼t4 period. At this time, the resonant current is equal to the excitation current, and the duty cycle is smaller.

Since the peak excitation current is positively correlated with the output voltage when the converter is running under light load conditions, the output current needs to be reduced to achieve output voltage stability; however, the reduction of the output current will lead to the reduction of excitation current and thus affect the duty cycle of PWM control pulses, so the duty cycle is reduced. At this time, the switching tubes Q_2 and Q_3 are difficult to achieve ZVS, and the EMI characteristics and stability of the system are impaired.

C. PWM-BURST HYBRID CONTROL

The analysis of PWM control and burst control indicates that:

1. In light load operations, the duty cycle of PWM control follows the decrease of excitation current, which cannot provide all the energy required by the switching tube ZVS.

2. Similarly, the resonant current of burst control is too large at a light load, which greatly affects the conversion efficiency of the system.

Therefore, the two control methods are combined so that the PWM comparator generates PWM pulses in the burst-on period. The excessive resonant current in the burst-on time is used to provide energy for the PWM control ZVS to compensate for the defect that the PWM control excitation current is too small. Meanwhile, since some of the energy of burst control is transferred to PWM control, the energy transformed to the output side is reduced, and the output voltage ripple is also reduced; the EMI characteristics are improved, and the output voltage range is widened.

Both control methods use double closed-loop stacked PI control. The outer is the voltage loop PI controller to introduce negative voltage feedback; the inner current loop PI controller will feedback current input compared with the current amplitude, to achieve the feedback voltage on the current amplitude control. Then, the PWM generator's logic generates PWM pulses at a certain frequency and in a visible duty cycle. Similarly, after the voltage and current double-loop control, the on-off signal of burst control is generated. Finally, the two signals are superimposed by a logic and gate circuit to form a PWM-Burst control pulse.

When the converter operates in burst control, the control of its frequency does not affect the converter's operating state, and the converter is only related to the burst control duty cycle. Meanwhile, a certain periodic current change during the burst control conduction period is only related to the system parameters and the current output voltage [14]. In the early design stages, the burst control frequency should be set as the rated operating frequency of the converter. When the D_{PWM} is set to 0.5 in the initial state, the D_{PWM} varies with the output voltage as the converter charging process proceeds. This variation is unpredictable and nonlinear because the equivalent load size of the electric vehicle power pack is variable and the required charging voltage varies from vehicle to vehicle. In this case, it is impossible to fit the D_{PWM} value linearly. Theoretically, the minimum duty cycle at different

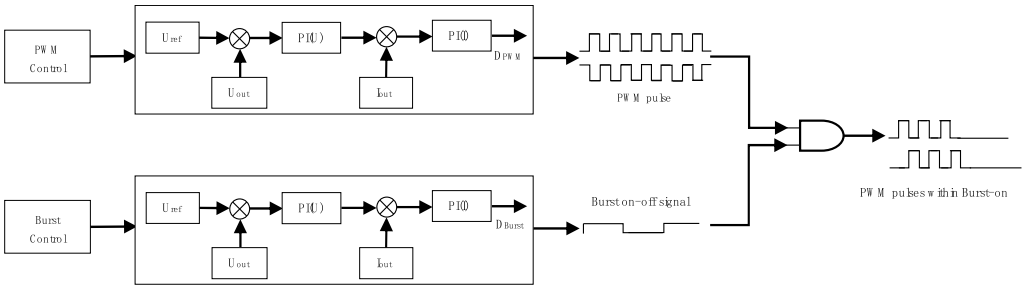

FIGURE 4. The principle diagram of PWM-Burst control.

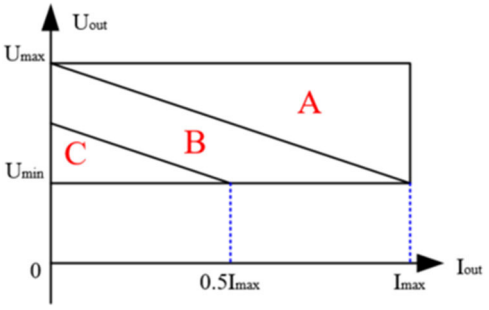

FIGURE 5. Schematic diagram of working mode.

output voltage points can be collected in the design process according to the converter design specifications, and the nearest two voltage values of this voltage can be found by checking the table with the minimum duty cycle corresponding to the output voltage and calculating the D_{PWM} value using the linear difference method [14].

D. PFM+PWM-BURST HYBRID CONTROL

The LLC resonant converter using conventional PFM-PWM control is mostly divided into two cases: PFM at light load or PFM at heavy load, and PWM at light load or PWM at heavy load. Both PFM and PWM control can achieve the basic requirements of the converter during the heavy load operation, but the ZVS characteristics of PWM control are impaired at light load, and the output voltage ripple of PFM control is large, so the combination of PFM-Burst control is considered in Section 2.3. Therefore, this paper considers combining PWM-Burst control under light load and PFM control under heavy load.

When charging electric vehicles, due to the limitations of models and power pack types, different electric vehicles correspond to different charging voltages and charging currents; even the charging voltage and charging current of the same model under different power consumption conditions may vary during multiple charging. Considering this situation, the output voltage range and output current range are chosen to define different working modes, as shown in Figure 6. In this figure, U_{max} and U_{min} indicate the maximum and minimum output voltage, and I_{max} and I_{min} indicate the maximum and minimum output current, respectively.

1. Area A: The output voltage U_{out} and output current I_{out} in this area are located in the following areas:

$$U_{out} > U_{min} + \left(I - \frac{I_{out}}{I_{max}}\right)(U_{max} - U_{min}) \tag{3}$$

$$0 < I_{out} < I_{max} \tag{4}$$

Under the premise that the charging equipment power is determined, this area belongs to the heavy load operation situation. In this case, PFM control is used, and PFM pulses with a fixed duty cycle and adjustable frequency are used as the drive signal of the full-bridge LLC resonant converter.

2. Area B: In this case, the converter runs between light load and heavy load, close to half load. At this time, the output voltage U_{out} and output current I_{out} are taken as follows:

$$\begin{pmatrix} U_{min} + \left(0.5 - \frac{I_{out}}{I_{max}}\right)(U_{max} - U_{min}) \leqslant U_{out} \\ \leqslant U_{min} + \left(1 - \frac{I_{out}}{I_{max}}\right)(U_{max} - U_{min}) \end{pmatrix} \tag{5}$$

$$0.5I_{max} \leqslant I_{out} \leqslant I_{max} \tag{6}$$

In this case, PWM control is used, and PWM pulses with a fixed frequency of 150 kHz and an adjustable duty cycle are used as the driving signals for the upper and lower bridge arms of the full-bridge LLC resonant converter, with the driving signal duty cycle varying with the load and output voltage.

3. Area C: the output voltage Uout and output current Iout take the value of this region:

$$U_{out} < U_{min} + \left(0.5 - \frac{I_{out}}{I_{max}}\right)(U_{max} - U_{min}) \tag{7}$$

$$0 < I_{out} < 0.5I_{max} \tag{8}$$

In this case, the PWM-Burst control method is adopted, and intermittent PWM pulses with a fixed frequency and an adjustable duty cycle are taken as the drive signal to drive the primary side switch tubes of the full-bridge LLC resonant converter.

IV. PARAMETER DESIGN

This section proposes the objective function and constraints for optimizing the resonance parameters of the converter based on the above control strategy and uses the quantum particle swarm algorithm to design the resonance parameters.

A. OBJECTIVE FUNCTION

The overall loss of the LLC resonant converter is negatively related to the conversion efficiency of the system, i.e., the essence of maximizing the conversion efficiency is to minimize the system loss rate. Then, the objective function can be expressed as the minimum system loss to achieve output voltage with a wider range under different resonant parameter selection values, with any preset range of input voltage, switching frequency, and load resistance, as shown below:

$$minfitness\,(L_m, L_r, C_r) = \sum_{U_{in}\in U_s} \sum_{f\in f_{ab}} \sum_{R_{eq}\in R_s} \eta \tag{9}$$

$$\eta = \frac{E_{loss}}{P_{out}} \tag{10}$$

where, P_{out} represents the output power of the converter, and E_{loss} represents the overall loss of the converter.

B. CONSTRAINTS

1) DC GAIN CONSTRAINT

The converter should operate in the inductive region, so the DC gain constraint is expressed as:

$$G(Q_{min}, 2\pi f_{min}) \geqslant G(Q_{min}, 2\pi f_r) \tag{11}$$

Where

$$G(s) = \frac{1}{\sqrt{\left(1 + k\left(1 - \frac{1}{f_n^2}\right)\right)^2 + \left(f_n - \frac{1}{f_n}\right)^2 Q^2}} \tag{12}$$

where, K represents the ratio of resonant inductance to excitation inductance, i.e., the inductance normalized quantity; Q represents the resonant converter quality factor; f_n represents the normalized operating switching frequency.

Meanwhile, due to the limited operating switching frequency range of the converter, to ensure that the converter can complete the charging process normally, the DC gain also needs to meet:

$$U_{out-max} \leqslant U_{in-min} G(Q_{max}, f_{n-min}) \tag{13}$$

$$U_{out-min} \geqslant U_{in-max} G(Q_{min}, f_{n-max}) \tag{14}$$

2) ZVS CONSTRAINT

The ZVS requires two necessary conditions, namely, inductive impedance and a large enough resonant current peak, to make the junction voltage drop to 0 at both ends of the switching tube during the dead time:

$$tan\theta = \frac{Z_{nI}}{Z_{nR}} \geqslant 0 \tag{15}$$

$$\frac{1}{2}(L_m + L_r) I_{m-peak}^2 \geqslant \frac{1}{2} C_{oss} U_{in}^2 \tag{16}$$

$$L_m < \frac{T_s T_{dead}}{16 C_{oss}} \tag{17}$$

where: Z_{nR} is the real part of the input impedance of the resonant network,

Z_{nI} is the imaginary part of the input impedance of the resonant network,

$tan\theta$ is the impedance angle,

I_{m-peak} is the peak excitation inductance current,

C_{oss} is the switching tube junction capacitance,

T_s is the switching period,

and T_{dead} is the dead time.

3) OPERATING FREQUENCY CONSTRAINT

The operating frequency of the switch should satisfy:

$$\begin{cases} f_s \leqslant f_{min} \leqslant f_r \\ f_{max} \geqslant f_r \end{cases} \tag{18}$$

where f_s and f_r denote the two resonant operating frequencies of the resonant network, f_{max} denotes the maximum operating frequency, and f_{min} denotes the minimum operating frequency.

4) BATTERY PACK LOAD CONSTRAINT

Considering the battery pack load charging condition, if the converter can complete the charging behavior at the worst working point, the converter can complete all charging behaviors under this load. Therefore, the battery pack load constraint can be expressed as:

$$L_{m-vile} \leqslant \frac{T_{dead}}{8\pi f_r C_{oss}} \sqrt{\left(l + \frac{1}{k}\right) G_{min}^2 - \frac{1}{k\,(l+k)}} \tag{19}$$

5) CONTROL CONDITION CONSTRAINT

The peak resonant current is set to I_{r-max}. To prevent the occurrence of overcurrent protection caused by excessive resonant current, the resonant current at any moment in the whole working process of the converter should be less than the peak resonant current. Thus, the resonant current peak I_{r-max} satisfies.

$$I_{r-max} = \sqrt{2} I_{r-rms} = \frac{U_{out}}{4nR_o} \sqrt{\frac{n^2 R_o^2 T_s^2}{L_m^2} + 4\pi^2} \tag{20}$$

Meanwhile, it must be ensured that the burst control provides sufficient resonant current for the switching tube junction capacitance in the burst-on period to achieve ZVS under light load conditions for all switching tubes. Defining the minimum current for the switching tube ZVS achievement as I_{r-zvs}, we have:

$$I_{r-zvs} = \frac{2 U_{in} C_{oss}}{T_{dead}} \tag{21}$$

C. ALGORITHM FLOW

Step 1: Initialize the design specifications of the LLC resonant converter

The initial parameters of the converter usually include input voltage range, output voltage range, switching operating frequency range, load resistance range, resonant frequency, power rating, etc. Meanwhile, the switching tube junction capacitance, drive signal period, and dead time need to be preset.

Step 2: Initialize the population particle position

Call the fitness function to calculate the fitness values of all particles within the design range of resonance parameters and determine the particle range.

Step 3: Initialize the parameters of the QPSO algorithm and generate N sets of particles randomly.

TABLE 1. The parameters of the QPSO algorithm.

QPSO algorithm parameters	Set value
Number of iterations K	1000
Number of particles N	30
Particle Dimension	3

N particles are randomly generated, their positions are denoted as (L_m, L_r, C_r), and the initialization is set as $l = 0, i = l, 2, \cdots, N$.

Step 4: Calculate the current fitness values of N sets of resonance parameters and update the individual average optimal position M_{best}, individual optimal position P_{best} and global optimal position g_{best}.

Calculate the current fitness value of N sets of resonance parameters at the k-th iteration, and compare it with the minimum fitness value of the individuals in the previous iterations. Then, compare the current adaptation minima of each particle with the global adaptation minima: if it is better, update the current global optimal position g_{best} keep the global adaptation minima, and determine the individual average optimal position M_{best}.

Step 5: Update the particle position

Calculate the particle positions for the next iteration, where the control parameter α uses an adaptive linear decay factor.

$$\alpha = \frac{l}{2} + \frac{K-k}{2K} \tag{22}$$

At the beginning of the iteration, α is larger, and the particle search ability is stronger; at the end of the iteration, α is smaller, and the particle search ability is weakened; however, the particles tend to be stable at this time, so the whole algorithm can achieve stable convergence.

Step 6: determine whether the number of iterations is reached. If it is reached, then go to the next step; otherwise, return to Step 4 and re-enter the optimization process.

Step 7: The global optimal position of the current particle is output as the optimal result, and the algorithm execution is completed.

D. OPTIMIZATION RESULTS

Using the QPSO algorithm to determine resonance parameters, the final optimal design results are listed in Table 2.

Figure 6 shows the convergence curve of the fitness function during the execution of the QPSO algorithm. Taking the minimum relative loss rate as the fitness function, its value decreases rapidly as the number of iterations increases. The reduction rate decreases until about 500 iterations when the relative loss rate fluctuates between 0.1 and 0.2; the relative loss rate stabilizes around 0.1 until about 650 iterations. The convergence of the algorithm can also be observed from the curve. If the number of iterations is further increased, the parameter values will be more accurate.

TABLE 2. The design results of resonance parameter optimization.

Resonance parameters	Optimal design results
Excitation inductance L_m	140μH
Resonant inductors L_r	21μH
Resonant Capacitor C_r	94nF

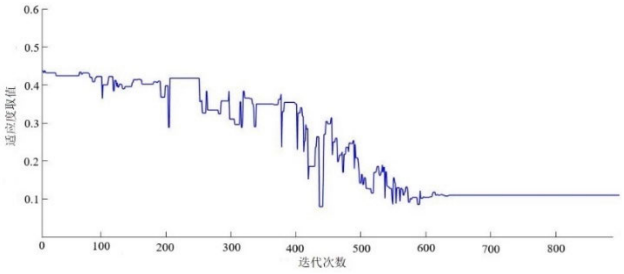

FIGURE 6. Fitness function convergence curve.

V. SIMULATION RESULTS

A full-bridge LLC resonant converter rated at 15 kW is modeled in Matlab-Simulink, and the design method of the resonant network parameters is derived from Section III.

From the above output voltage range, it can be seen that:

$$200\text{V} \leqslant U_{out} \leqslant 750\text{V} \tag{23}$$

$$0 < I_{out} \leqslant 75\text{A} \tag{24}$$

$$\begin{cases} \text{A:} U_{out} > 750 - \dfrac{21 I_{out}}{5}, 0 < I_{out} < 75\text{A} \\ \text{B:} 475 - \dfrac{21 I_{out}}{5} \leqslant U_{out} \leqslant 750 - \dfrac{21 I_{out}}{5}, 37.5\text{A} \leqslant I_{out} \leqslant 75\text{A} \\ \text{C:} U_{out} < 475 - \dfrac{21 I_{out}}{5}, 0 < I_{out} < 37.5\text{A} \end{cases} \tag{25}$$

The output voltage and current in the charging process are determined by the load of the power battery pack, which is highly random. To recreate the charging process of electric vehicles to the maximum extent, Uout is randomly taken, and the output situation is simulated and tested separately to verify whether the wide output voltage range is achieved with this control strategy. The simulation test diagrams from top to bottom are drive signal, resonant current and excitation current, output current, and output voltage.

The simulation results under different operating conditions are shown in Figure 7. They are the simulated waveforms at an output power of 200V, 460V, 600V, and 750V, and the corresponding output currents are 12A, 27.58 A, 40.8A, and 45 A, respectively. From these simulation test diagrams,

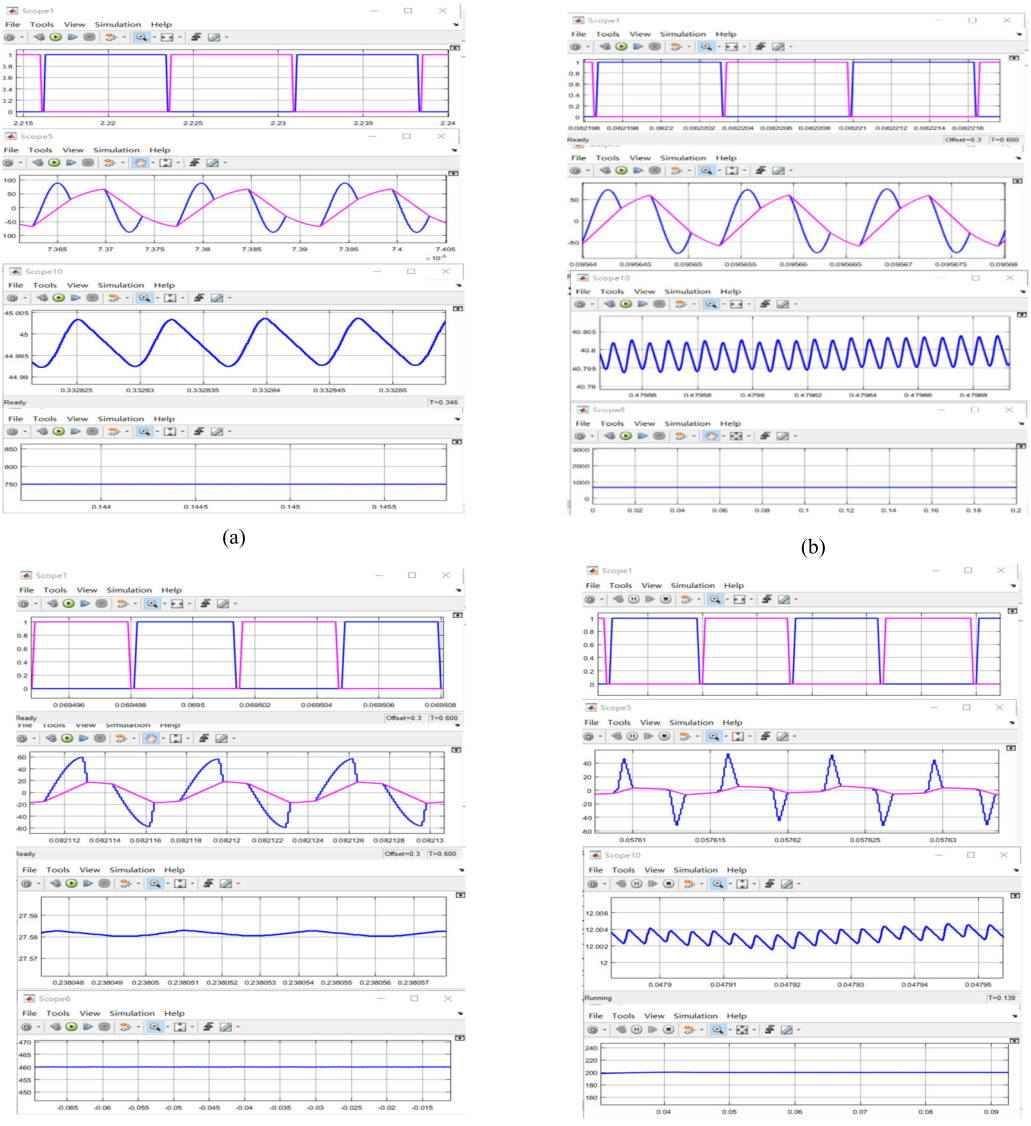

FIGURE 7. Simulation results. (a) 750V output voltage. (b) 600V output voltage. (c) 460V output voltage. (d) 200V output voltage.

it can be observed that the proposed converter can achieve a stable output, and the operating pattern is the same as the previous analysis result. As shown in Figure 7(c)(d), the issue of uncontrolled converter voltage is addressed under light load. At this time, for the converter working in region C, the pulsation error is negligible. The PWM-Burst control is used to provide the converter with a drive signal of PWM pulses in the burst-on period.

The simulation indicates that the PFM+PWM-Burst control strategy can enable the full-bridge LLC resonant converter to work in the normal output state based on electric vehicle charging equipment, realize ZVS effectively under all load conditions, reduce circuit losses, and effectively widen the output voltage range, thereby verifying the feasibility and

TABLE 3. The specifications of the full-bridge LLC resonant converter model.

Initial Parameters	Design Specifications
Excitation inductance Lm	140mH
Resonant inductors Lr	21mH
Resonant Capacitor Cr	94nF
Rated operating frequency	150kHz
Input Voltage Range	350~400V
Output Voltage Range	200~750V
Switching operating frequency range	60~150kHz

rationality of the control strategy. Next, the control strategy is used in the full-bridge LLC resonant converter prototype for experimental analysis.

VI. EXPERIMENTAL RESULTS

An experimental prototype was designed to verify the operating principle and performance of the proposed converter, as shown in Figure 8. The output voltage range is 200-500V. It has a resonant frequency of 153 kHz and a switching frequency range of 100-250 kHz, as shown in Table 4.

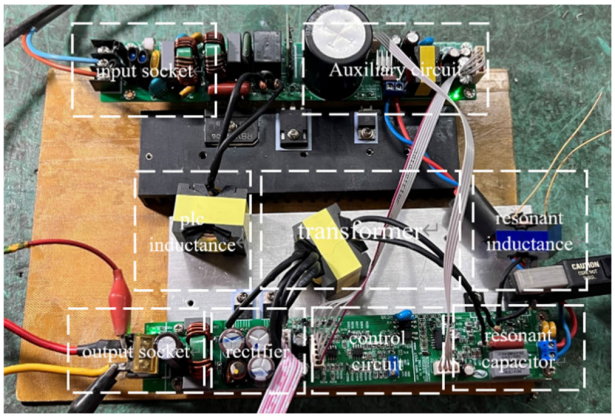

FIGURE 8. Laboratory prototype.

TABLE 4. Full-bridge LLC resonant converter prototype.

Initial Parameters	Design specifications
Excitation inductance Lm	140μH
Resonant inductors Lr	21μH
Resonant Capacitor Cr	94nF
Transformer turns ratio	7:6
Output power	1kW
Rated operating frequency range	100~250kHz
Input Voltage Range	350~400V
Output Voltage Range	200~500V

Figure 9 illustrates the gate voltage of the MOSFETs in the whole switching network of the proposed converter. The rise tie of the gate voltage is 2us, which satisfies the requirement of frequency modulation.

Figure 10 shows the output voltage waveform of the LLC converter when only PWM control is used. It can be observed that with PWM control alone, the switching process of the transistors results in hard switching, causing voltage spikes due to the abrupt changes in the transistor state.

Figure 11 shows the output voltage waveform of the LLC converter when PWM-burst control is used. There are voltage spikes only in the first switching cycle of Burst-on, and

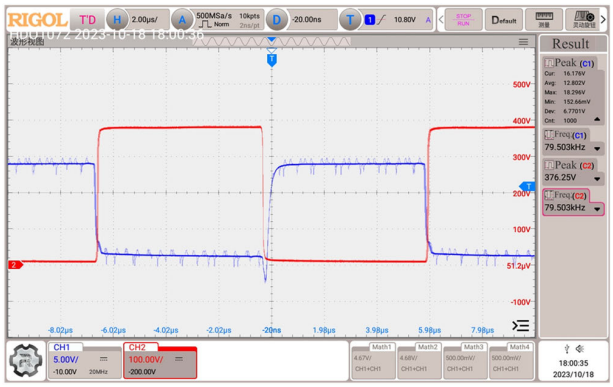

FIGURE 9. The gate voltage of the MOSFET for the switching network.

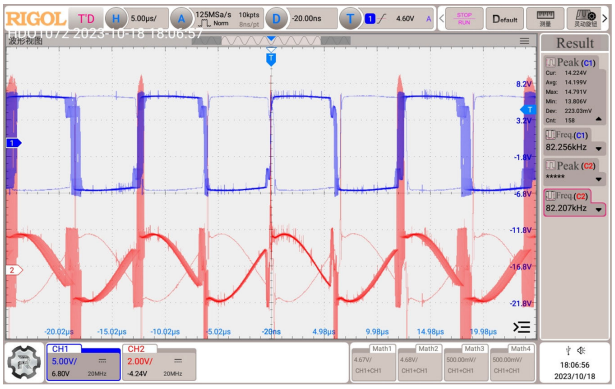

FIGURE 10. Waveforms with the PWM control.

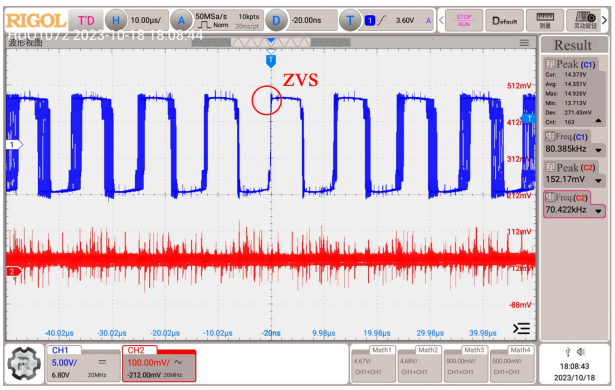

FIGURE 11. The waveforms with the PWM-burst control.

thereafter, soft switching is achieved, which improves the reliability of the system over a wide voltage output range.

Figure 12 shows the resonant current of the resonant tank of the proposed prototype for the switching network under different load conditions. Figure 12(a) shows the resonant current curve of the converter under light load, when the converter operates in region C. When the excitation current and the capacitor voltage of the switch junction complete the energy transfer process, the zero voltage of the switch is on, and the dead time is over. Under this load condition, the converter can achieve a stable DC output.

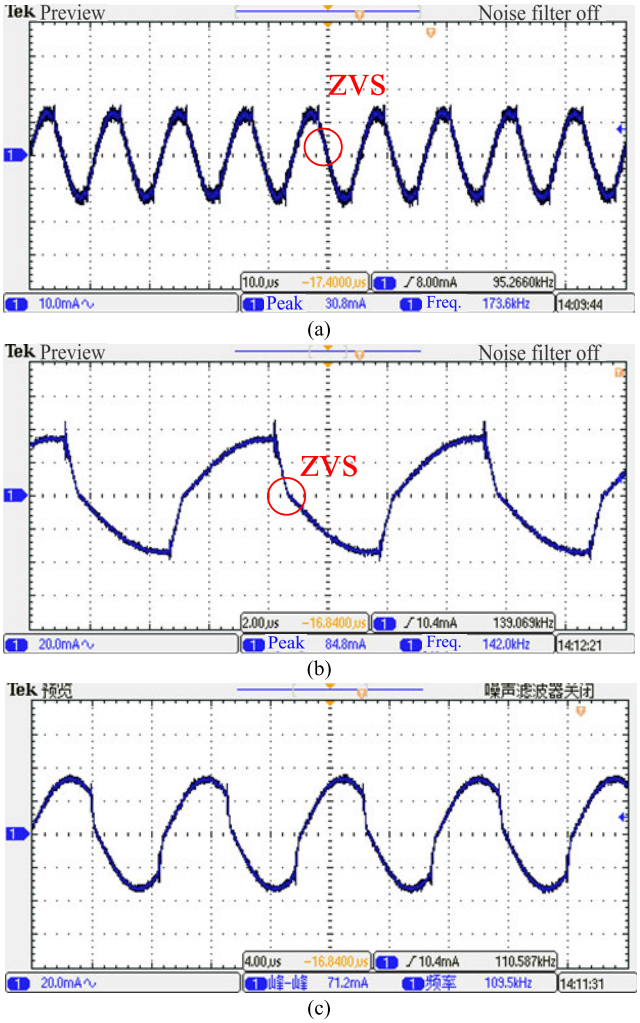

FIGURE 12. (a) The resonant current waveform under light load. (b) The resonant current waveform under half load. (c) The resonant current waveform under full load.

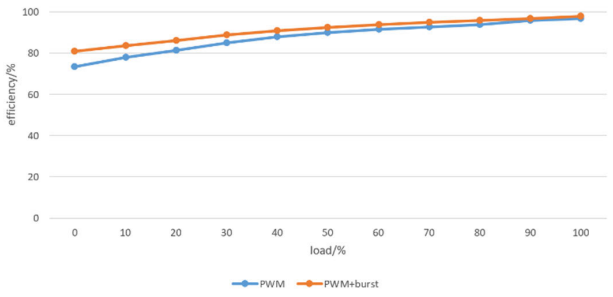

FIGURE 13. Efficiency comparison between the PWM and PWM-Burst hybrid control strategy.

Figure 12(b) shows the resonant current curve of the converter under half load. When the converter is working in region B, the excitation current and resonant current are equal to realize ZVS. Under this load condition, the converter can also achieve stable DC output. Figure 12(c) shows the resonant current curve of the converter under full load. When the converter works in region A, the excitation current is equal to the resonant current and can achieve ZVS for a period of time. Under this load condition, the converter can also achieve stable DC output.

By applying the PFM+PWM-Burst control strategy to the full-bridge LLC resonant converter prototype, the control strategy can realize output voltage control under different load conditions, and the direct connection between the control area division and the output helps to widen the output voltage range, thereby reducing the loss caused by the failure to achieve ZVS in the previous light load control and realizing ZVS under the full load condition. This confirms the applicability of the control strategy.

In Figure 13, the efficiency of the proposed PWM-burst method and traditional PWM are shown under full load conditions. When the load is below 70%, PWM cannot achieve ideal voltage regulation, while PWM-burst can. Under heavy load conditions, the efficiency of PWM-burst is also higher than that of PWM.

VII. CONCLUSION

This paper introduces the parameter design method of the commonly used full bridge LLC resonant converter in the DC/DC module of charging equipment, and proposes a hybrid control method PWM control with Burst control. The following conclusions are drawn:

(1) PWM control can effectively reduce the current stress during the Burst-on period, while Burst control can provide sufficient current during the Burst-on period to enable high-frequency soft switching of the switches. The combination of the two methods allows the converter to maintain reliability based on a wide range of voltage outputs.

(2) The current variation during the Burst-on period is only related to the difference between the input and output voltages and the resonant cavity parameters, and is independent of the load parameters. Therefore, the optimization of the resonant cavity parameters does not need to consider load changes, reducing the complexity of parameter design.

The experiment has verified the effectiveness of the described method and the correctness of the analysis.

REFERENCES

[1] Y. Wei and A. Mantooth, "An LLC converter with fixed switching frequency operation for renewable energy applications," in *Proc. IEEE Transp. Electrific. Conf. Expo (ITEC)*, Chicago, IL, USA, Jun. 2021, pp. 354–359.

[2] M. Abbasi, R. Emamalipour, K. Kanathipan, M. A. M. Cheema, and J. Lam, "A step-up reconfigurable multimode LLC converter module with extended high-efficiency range for wide voltage gain application in medium voltage DC grid systems," *IEEE Trans. Power Electron.*, vol. 37, no. 7, pp. 8118–8132, Jul. 2022, doi: 10.1109/TPEL.2022.3149294.

[3] X. Wu, R. Li, and X. Cai, "A wide output voltage range LLC resonant converter based on topology reconfiguration method," *IEEE J. Emerg. Sel. Topics Power Electron.*, vol. 10, no. 1, pp. 969–983, Feb. 2022.

[4] Z. Zhang, C. Liu, M. Wang, Y. Si, Y. Liu, and Q. Lei, "High-efficiency high-power-density CLLC resonant converter with low-stray-capacitance and well-heat-dissipated planar transformer for EV on-board charger," *IEEE Trans. Power Electron.*, vol. 35, no. 10, pp. 10831–10851, Oct. 2020.

[5] H. Park, M. Kim, H. Kim, and J. Jung, "Design methodology of tightly regulated dual-output LLC resonant converter using PFM-APWM hybrid control method," *Energies*, vol. 12, no. 11, p. 2146, Jun. 2019.

[6] R. G. Kumari and P. Sravani, "Analysis of uni-directional and bi-directional LLC resonant converter for battery charger application in electric vehicle," *J. Phys., Conf.*, vol. 1172, Mar. 2019, Art. no. 012098.
[7] T. Jun, L. I. Facheng, L. I. Xiang, and Y. Xingchen, "Loss analysis and optimization design of half-bridge LLC resonant converter," *IOP Conf. Ser., Mater. Sci. Eng.*, vol. 533, May 2019, Art. no. 012017.
[8] S. A. Arshadi, M. Ordonez, W. Eberle, M. Craciun, and C. Botting, "Three-phase LLC battery charger: Wide regulation and improved light-load operation," *IEEE Trans. Power Electron.*, vol. 36, no. 2, pp. 1519–1531, Feb. 2021.
[9] H.-N. Vu and W. Choi, "A novel dual full-bridge LLC resonant converter for CC and CV charges of batteries for electric vehicles," *IEEE Trans. Ind. Electron.*, vol. 65, no. 3, pp. 2212–2225, Mar. 2018, doi: 10.1109/TIE.2017.2739705.
[10] P. Zheng and J. Bauman, "High efficiency bidirectional LLC+C resonant converter with parallel transformers for solar-charged electric vehicles," *IEEE Trans. Transp. Electrific.*, vol. 9, no. 1, pp. 1428–1442, Mar. 2023, doi: 10.1109/TTE.2022.3199157.
[11] J.-P. He, J.-Y. Zhang, and H.-F. Ma, "Design of a bi-directional full bridge LLC resonant converter with a higher normalized voltage gain under backward mode," in *Proc. 19th Eur. Conf. Power Electron. Appl.*, Warsaw, Poland, 2017, pp. 1–9, doi: 10.23919/EPE17ECCEEurope.2017.8098974.
[12] J. Gao, J. Zhang, Q. Song, Z. Zhu, and L. Qian, "An LLC resonant single-stage inverter with high-frequency link and soft-switching," *IEEE J. Emerg. Sel. Topics Power Electron.*, vol. 10, no. 3, pp. 2959–2974, Jun. 2022, doi: 10.1109/JESTPE.2021.3123345.
[13] H. Xun, H. Shen, and W. Chen, "Efficiency optimization strategy of LLC resonant converter based on hybrid PWM and PFM digital control mode," *J. Phys., Conf.*, vol. 1941, no. 1, Jun. 2021, Art. no. 012023.
[14] U. Mumtahina and P. J. Wolfs, "Multimode optimization of the phase-shifted LLC series resonant converter," *IEEE Trans. Power Electron.*, vol. 33, no. 12, pp. 10478–10489, Dec. 2018.
[15] T. Zhu, F. Zhuo, F. Zhao, F. Wang, H. Yi, and T. Zhao, "Optimization of extended phase-shift control for full-bridge CLLC resonant converter with improved light-load efficiency," *IEEE Trans. Power Electron.*, vol. 35, no. 10, pp. 11129–11142, Oct. 2020, doi: 10.1109/TPEL.2020.2978419.
[16] M. Saadati and A. Ghayebloo, "A new detailed loss model and design approach for LLC resonant converter with phase shift control to overall optimization of converter loss at whole battery charging process," *Int. J. Circuit Theory Appl.*, vol. 50, no. 11, pp. 3763–3787, Nov. 2022.
[17] Y. Zhou, X. He, and L. Sheng, "Full-bridge resonant converter with hybrid control for wide input voltage range applications," *J. Power Electron.*, vol. 21, no. 1, pp. 269–281, Jan. 2021.
[18] B. Xue, H. Wang, J. Liang, Q. Cao, and Z. Li, "Phase-shift modulated interleaved LLC converter with ultrawide output voltage range," *IEEE Trans. Power Electron.*, vol. 36, no. 1, pp. 493–503, Jan. 2021.
[19] Z. Hu, Y. Qiu, L. Wang, and Y.-F. Liu, "An interleaved LLC resonant converter operating at constant switching frequency," *IEEE Trans. Power Electron.*, vol. 29, no. 6, pp. 2931–2943, Jun. 2014.
[20] S. A. Arshadi, M. Ordonez, M. Mohammadi, and W. Eberle, "Efficiency improvement of three-phase LLC resonant converter using phase shedding," in *Proc. IEEE Energy Convers. Congr. Expo. (ECCE)*, Cincinnati, OH, USA, Oct. 2017, pp. 3771–3775.
[21] L. Shi, B. Liu, and S. Duan, "Burst-mode and phase-shift hybrid control method of LLC converters for wide output range applications," *IEEE Trans. Ind. Electron.*, vol. 67, no. 2, pp. 1013–1023, Feb. 2020.
[22] S. Zhao, J. Xu, and O. Trescases, "Burst-mode resonant LLC converter for an LED luminaire with integrated visible light communication for smart buildings," *IEEE Trans. Power Electron.*, vol. 29, no. 8, pp. 4392–4402, Aug. 2014.
[23] N. Shafiei, M. Ordonez, M. Craciun, C. Botting, and M. Edington, "Burst mode elimination in high-power *LLC* resonant battery charger for electric vehicles," *IEEE Trans. Power Electron.*, vol. 31, no. 2, pp. 1173–1188, Feb. 2016.

YUNTAO YUE received the M.S. and Ph.D. degrees in power electronics from China University of Mining and Technology, Beijing, China, in 2003 and 2006, respectively. Since 2007, he has been an Associate Professor and the Dean of the School of Electrical and Information Engineering, Beijing University of Civil Engineering and Architecture. His research interests include motor drives, power electronics and power drives, pulse width mode converters, and microprocessor applications.

YUFAN LIU was born in Beijing, China, in 1999. She received the B.S. degree from Beijing University of Civil Engineering and Architecture, Beijing, in 2021, where she is currently pursuing the M.S. degree in electrical engineering.

Her research interests include modeling and control of bidirectional dc–dc converters.

JIARAN ZHANG received the Ph.D. degree from the Department of Information and Electrical Engineering, China Agricultural University. She is currently a Lecturer with the School of Electrical and Information Engineering, Beijing University of Civil Engineering and Architecture. Her research interests include sensors and detection techniques for food freshness.

HONGWEI ZHAO received the B.S. degree in electrical and information engineering from Beijing University of Civil Engineering and Architecture, Beijing, China, in 2022, where she is currently pursuing the M.S. degree in electrical engineering.

Her research interests include dc–dc converters and electrical power systems.

JIN YANG received the B.S. degree in electrical and information engineering from Beijing University of Civil Engineering and Architecture, Beijing, China, in 2022, where she is currently pursuing the M.S. degree in electrical engineering. Her research interests include sensors and electrical power systems.